IEEE Photonics Journal
An IEEE Photonics Society Publication

Open Access

Study on Transmission and Output Polarization Characteristics of a First-Order Lyot-Type Fiber Comb Filter Using Polarization-Diversity Loop

Volume 7, Number 4, August 2015

Songhyun Jo
Youngho Kim
Yong Wook Lee

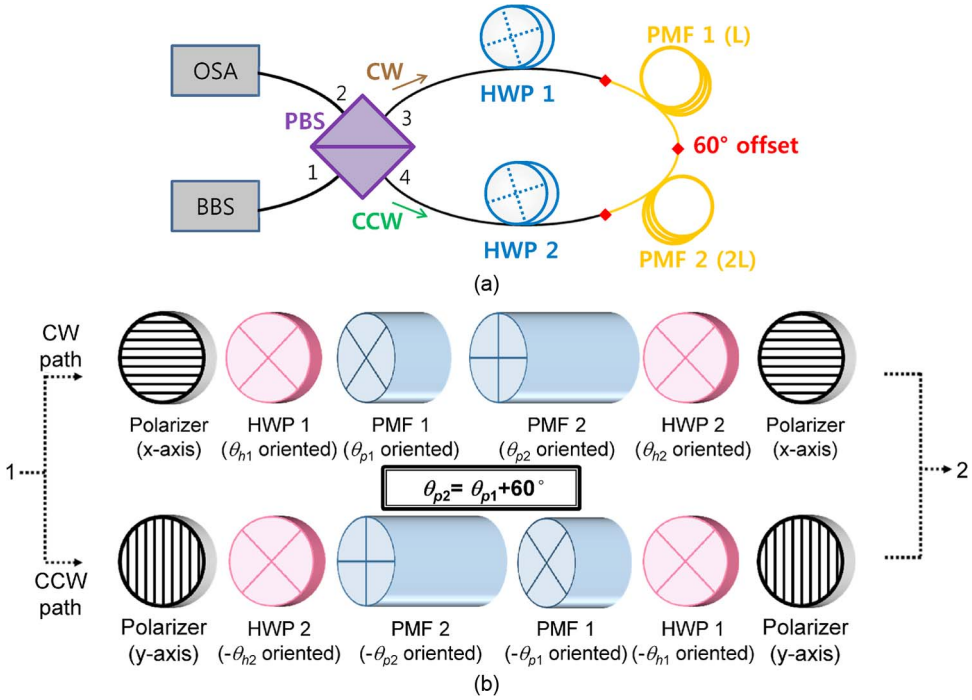

DOI: 10.1109/JPHOT.2015.2450998
1943-0655

Study on Transmission and Output Polarization Characteristics of a First-Order Lyot-Type Fiber Comb Filter Using Polarization-Diversity Loop

Songhyun Jo,[1] Youngho Kim,[2] and Yong Wook Lee[1,3]

[1]School of Interdisciplinary Program of Biomedical Mechanical and Electrical Engineering, Pukyong National University, Busan 608-737, Korea
[2]Nano Fusion Technology Research Center, Korea Electrotechnology Research Institute, Changwon 642-120, Korea
[3]School of Electrical Engineering, Pukyong National University, Busan 608-737, Korea

DOI: 10.1109/JPHOT.2015.2450998

Manuscript received May 31, 2015; accepted June 24, 2015. Date of publication June 30, 2015; date of current version July 10, 2015. This work was supported by the National Research Foundation of Korea under Grant 2013R1A2A2A01068390 funded by the Korean government (MSIP). Corresponding author: Y. W. Lee (e-mail: yongwook@pknu.ac.kr).

Abstract: A first-order Lyot-type fiber comb filter was fabricated by incorporating a polarization-diversity loop structure composed of a polarization beam splitter, two half-wave plates (HWPs), and two polarization-maintaining fiber (PMF) segments. One of the two PMF segments was two times longer than the other, and they were concatenated with a 60° offset between their principal axes. The transmission spectra and output polarization characteristics of the filter were theoretically predicted and experimentally verified. By proper control of the two HWPs, first-order transmission spectra could be obtained, including flat-top and lossy flat-top band modes, and the interleaving operation of the respective spectrum could be also achieved. This flat-top band mode spectrum showed a higher attenuation rate at the cutoff level, in comparison with that of the Solc-type filter. In particular, it was revealed that the output state of polarization of the filter was a periodical function of wavelength and that the evolution period was different, according to transmission band modes. With the help of a linear output polarizer, the specific portion of a passband could be passed or rejected by controlling input polarization. It was also theoretically predicted that the fine tuning of the passband center was possible within a specific wavelength range.

Index Terms: Fiber comb filter, Lyot filter, birefringence, polarization-diversity loop, polarization-maintaining fiber (PMF).

1. Introduction

A polarization-diversity loop structure (PDLS) that can form a Sagnac interferometer loop using a polarization beam splitter (PBS) has been used for achieving input polarization independence in nonlinear optical switching applications [1], [2]. This PDLS can also be employed to create comb spectra induced by polarization interference based on high birefringent elements and realize their wavelength switching [3], [4]. Switchable comb spectra can be utilized to optical pulse train generation [5]; high-speed wavelength routing [6]; optical label switching [7], [8]; and multiwavelength fiber lasers [9]–[12]. The absolute wavelength switching or tuning of multiwavelength filter

channels, which was not obtained in the conventional Sagnac birefringence filter (SBF) based on a fiber coupler [13], was demonstrated in polarization-independent fiber comb filters based on the PDLS [3], [4]. For high-order (flat-top or narrow band) comb spectra, Solc-type fiber comb filters were suggested by incorporating the PDLS [14], [15]. For example, a first-order Solc-type comb filter based on the PDLS utilizes two segments of polarization-maintaining fiber (PMF) of the same length, concatenated with an angle offset of 45° [14]. This Solc-type comb filter can provide high-order filtering functions such as filter transmittances exhibiting flat-top pass band and narrowband transmission spectra and also a switching capability that can make these high-order spectra be interleaved [14]. In the case of a Lyot-type comb filter, another filter structure for high-order comb spectra, a fiber coupler [16], [17] or 45°-tilted fiber gratings [18] were chosen for implementing Lyot-type comb filters, but their high-order transmission spectra were not fully investigated; moreover, they were fixed in the wavelength position. Recently, the PDLS was utilized for realizing a first-order [19] Lyot-type fiber filter [20]. The PDLS-based Lyot filter, which contained two PMF segments connected with a length ratio of 1 to 2 and an offset angle of 60° between their principal axes, showed flat-top pass bands and the capability of switching multiwavelength channels with high-order spectra. But its spectral characteristics including filter sharpness and, especially, output polarization leave some room for more rigorous and meaningful investigation.

In this paper, we studied the transmission and output polarization properties of a first-order Lyot-type fiber comb filter based on the PDLS. The first-order Lyot-type filter, composed of a PBS, two half-wave plates (HWPs), and two PMF segments, was fabricated for the investigation. Two PMF segments were concatenated with a 60° offset between their principal axes, and one of them was two times longer than the other. The transmittance of the fabricated filter was theoretically analyzed, and the theoretical prediction was verified by experimental demonstration. By controlling two HWPs, the filter could operate in a flat-top or a lossy flat-top band mode, and its multiwavelength channels could be interleaved in both modes, which could not be obtained in the previous Lyot-Sagnac comb filter [16]. In addition, the filter showed sharper transition between pass and stop bands in comparison with a PDLS-based Solc-type comb filter with the same order. In particular, the output state of polarization (SOP) of the fabricated filter was examined in a wavelength range within one channel bandwidth (0.8 nm). The calculated spectral variation of the output SOP $(\mathrm{SOP}_{\mathrm{out}})$ was also verified through experiments using a coherent light source and an output linear polarizer (analyzer). The $\mathrm{SOP}_{\mathrm{out}}$ of the filter was a periodic function of wavelength, showing wavelength-dependent evolution. When considering polarization evolution on the Poincare sphere, this wavelength dependence made a surface point on the sphere indicating the $\mathrm{SOP}_{\mathrm{out}}$ move rotating in a clockwise direction around the axis of linear horizontal polarization (LHP) with increasing wavelength. The evolution period was different according to transmission band modes. For flat-top and lossy flat-top band modes, the spectral periods of the evolution were the channel spacing of the filter and its half, respectively. Irrespective of transmission band modes, however, an $\mathrm{SOP}_{\mathrm{out}}$ at the pass band center (transmission maximum) was the same as an input SOP $(\mathrm{SOP}_{\mathrm{in}})$. With the help of the analyzer, some spectral portion of a channel could be passed or rejected by controlling input polarization. Theoretically, the fine and continuous tuning of the pass band center was possible in a specific wavelength range corresponding to ~12.81% of the channel spacing with an insertion loss (IL) less than 0.023 dB and a side-mode suppression ratio (SMSR) more than 30 dB. In Sections 2 and 3, the filter transmittance will be analyzed theoretically and experimentally, respectively. Then, the spectral variation of $\mathrm{SOP}_{\mathrm{out}}$'s of the filter will be investigated in Section 4. Finally, a brief summary will be given in Section 5.

2. Theoretical Analysis on Filter Operation

Fig. 1(a) shows the schematic diagram of the fabricated Lyot-type fiber comb filter. The fabricated filter consists of a PBS, two HWPs, and two PMF segments concatenated with a 60° offset between their principal axes, and two HWPs are placed at both ends of two PMF segments to control the SOP of light propagating through the polarization-diversity loop. To implement Lyot-type birefringence combination, the length of the PMF 2 was tailored to be doubled,

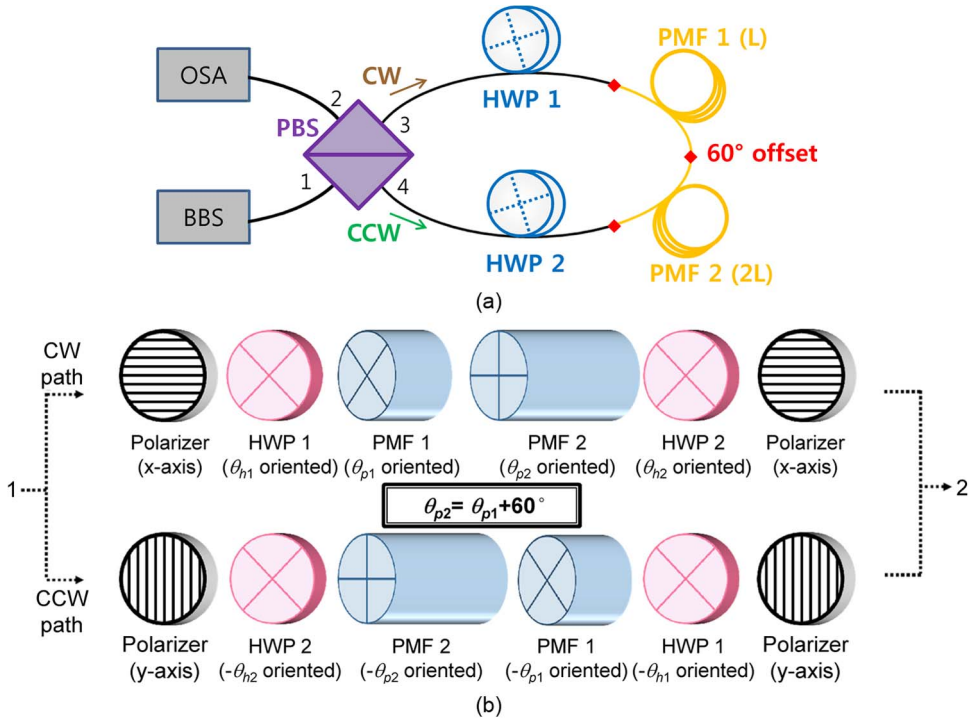

Fig. 1. (a) Schematic diagram of Lyot-type optical fiber comb filter based on PDLS and (b) light propagation paths within Lyot-type filter.

compared with that of the PMF 1 [16]. A broadband light source (BBS) emitting amplified spontaneous emission light and an optical spectrum analyzer (OSA), shown in Fig. 1(a), were utilized as an input light source and a spectrum monitoring instrument for the filter characterization, respectively. Input light entering the port 1 of the PBS is decomposed into two orthogonal linearly-polarized components. Linear horizontal and vertical polarization components, aligned along the horizontal (x) and vertical (y) axes of the PBS, circulate through the Sagnac loop of the PDLS in a clockwise (CW) direction and a counterclockwise (CCW) direction, respectively. As can be seen from Fig. 1 (b), light rotating along the CW path passes through the polarizer (from the port 1 to port 3 of the PBS), HWP 1, PMF 1, PMF 2, HWP 2, and the analyzer (from the port 4 to port 2 of the PBS), and light rotating along the CCW path the polarizer (from the port 1 to port 4), HWP 2, PMF 2, PMF 1, HWP 1, and the analyzer (from the port 3 to port 2) in turn. Light that returns to the PBS after traveling round the CW and CCW paths experiences linear horizontal and vertical polarizers, respectively, when it passes through the PBS. Linearly polarized components coming out of the PBS generate respective interference spectra of comb shape, as the PMF segments and the HWPs act as birefringence elements and polarization controllers, respectively. These respective interference spectra are simply superposed due to the orthogonality of their polarization states.

By incorporating Jones matrix formulation [21], theoretical transmittance of the filter can be obtained from the transfer matrix T of the filter. As shown in (1), the transfer matrix T is expressed as the algebraic sum of two transfer matrices T_{CW} and T_{CCW}. T_{CW} and T_{CCW} indicate filter transfer matrices when light rotates within the filter along CW and CCW paths, respectively.

$$
\begin{aligned}
T &= T_{CW} + T_{CCW} \\
T_{CW} &= \begin{bmatrix} 1 & 0 \\ 0 & 0 \end{bmatrix} T_{H2}(\theta_{h2}) T_{P2}(\theta_{p2}) T_{P1}(\theta_{p1}) T_{H1}(\theta_{h1}) \begin{bmatrix} 1 & 0 \\ 0 & 0 \end{bmatrix} \\
T_{CCW} &= \begin{bmatrix} 0 & 0 \\ 0 & 1 \end{bmatrix} T_{H1}(-\theta_{h1}) T_{P1}(-\theta_{p1}) T_{P2}(-\theta_{p2}) T_{H2}(-\theta_{h2}) \begin{bmatrix} 0 & 0 \\ 0 & 1 \end{bmatrix}
\end{aligned} \tag{1}
$$

TABLE 1

Four specific flat-top band transmission modes of Lyot-type filter

Transmission modes	Flat-top band mode (t_f)	Interleaved flat-top band mode ($t_{f,i}$)	Lossy flat-top band mode (t_{lf})	Interleaved lossy flat-top band mode ($t_{lf,i}$)
θ_{h1}	$(\theta_{p1} + \pi/4)/2$	$(\theta_{p1} - \pi/4)/2$	$(\theta_{p1} + 2\pi/17)/2$	$(\theta_{p1} - 2\pi/17)/2$
θ_{h2}	$(\theta_{p1} + \pi/4)/2$		$(\theta_{p1} - 2\pi/17)/2 + \pi/4$	

where T_{H1}, T_{H2}, T_{P1}, and T_{P2} are Jones transfer matrices of the HWP 1, HWP 2, PMF 1, and PMF 2 that have orientation angles of θ_{h1}, θ_{h2}, θ_{p1}, and θ_{p2}, respectively. As two PMF segments are spliced with an offset angle of 60°, $\theta_{p2} = \theta_{p1} + 60°$. The filter transmittance t can be derived from T and is given by

$$\begin{aligned} t = \Bigg[& \cos^2\left(\frac{\Gamma}{2}\right)\left\{\cos^2(\Gamma)\cos^2(2\theta_{h1} - 2\theta_{h2}) + \cos^2(2\theta_{h1} + 2\theta_{h2} - 2\theta_{p2})\sin^2(\Gamma)\right\} \\ & + \sin^2\left(\frac{\Gamma}{2}\right)\left\{\cos^2(\Gamma)\cos^2(2\theta_{h1} + 2\theta_{h2} - 2\theta_{p1}) + \sin^2(\Gamma)\cos^2(2\theta_{h1} - 2\theta_{h2} - 2\theta_{p1} + 2\theta_{p2})\right\} \\ & - \cos(\Gamma)\sin^2(\Gamma)\sin(4\theta_{h1} - 2\theta_{p1})\sin(4\theta_{h2} - 2\theta_{p2})\Bigg] \end{aligned} \tag{2}$$

where $\Gamma(= 2\pi BL/\lambda)$ generated due to the birefringence B and the length L of the PMF 1 (λ is the wavelength in vacuum) is a phase retardation difference between two orthogonally polarized modes along the principal axes of PMF. In this formulation, any IL due to optical components was not considered, and the phase retardation difference of the HWPs was assumed to be independent of wavelength.

If $[\theta_{h1}, \theta_{h2}]$ (orientation angles of the HWP 1 and HWP 2) are selected as one of four angle sets given by Table 1, it is possible to obtain one of four specific transmission spectra. Four specific transmission spectra include flat-top, interleaved flat-top, lossy flat-top, and interleaved lossy flat-top band transmission spectra. An interleaved spectrum implies a spectrally shifted version of the original spectrum, of which wavelength displacement is half a channel spacing (or an interference period). t_f, $t_{f,i}$, t_{lf}, and $t_{lf,i}$ indicate filter transmittances at these four specific transmission modes such as flat-top, interleaved flat-top, lossy flat-top, and interleaved lossy flat-top band modes, respectively, shown as

$$t_f = -\frac{1}{4}\cos^3\Gamma + \frac{3}{4}\cos\Gamma + \frac{1}{2} \tag{3}$$

$$t_{f,i} = \frac{1}{4}\cos^3\Gamma - \frac{3}{4}\cos\Gamma + \frac{1}{2} \tag{4}$$

$$t_{lf} = \alpha\cos^3\Gamma + \beta\cos^2\Gamma + \gamma\cos\Gamma + \delta \tag{5}$$

$$\begin{aligned} & t_{lf,i} = -\alpha\cos^3\Gamma - \beta\cos^2\Gamma - \gamma\cos\Gamma + \delta \\ & \left(\alpha = \frac{3}{8} + \frac{3}{4}\cos\frac{14}{51}\pi, \quad \beta = -\frac{3}{8} + \frac{\sqrt{3}}{4}\sin\frac{14}{51}\pi,\right. \\ & \left.\gamma = \frac{3}{8} + \frac{1}{4}\cos\frac{10}{51}\pi - \frac{1}{2}\cos\frac{7}{51}\pi, \quad \delta = \frac{5}{8} - \frac{1}{4}\cos\frac{10}{51}\pi\right). \end{aligned} \tag{6}$$

As shown in Fig. 1(b), light introduced into the filter undergoes the optical elements such as two polarizers, two HWPs, and two PMF segments along the CW or CCW propagation path. These four transmission modes are determined by the relationship between azimuthal orientation angles of two birefringent elements (i.e., PMF segments) and two polarizers shown in Fig. 1(b).

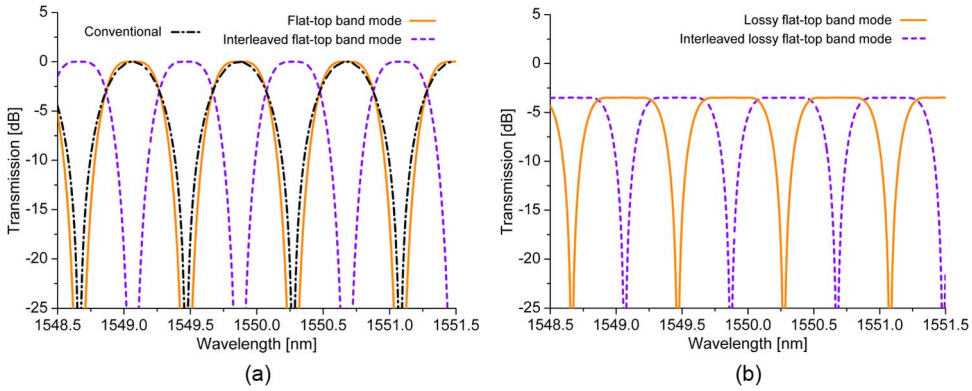

Fig. 2. Calculated transmission spectra of (a) flat-top and (b) lossy flat-top band modes. In both flat-top band modes, violet dashed lines indicate interleaved transmission spectra, in comparison with ones indicated as orange solid lines.

For example, a conventional zeroth order transmission mode can be obtained by placing one birefringent element between two polarizers with its fast-axis orientation angle set as $\pi/4$ with respect to the polarization plane of the polarizers. In the Lyot-type filter, the angle relationship between two PMF segments and two polarizers can be varied by adjusting the orientation angles of two HWPs (HWP 1 and HWP 2) inserted between them. This angle relationship in each transmission mode can be schematized using two PMF segments (PMF 1 and PMF 2) sandwiched by two polarizers, which is similar to the schematic diagrams shown in Fig. 1(b) except for the HWPs. In the case of the flat-top band mode, the polarization planes of input and output polarizers form the angles of $\pi/4$ and $-\pi/12$ in the CW path and the angles of $-5\pi/12$ and $-\pi/4$ in the CCW path, respectively, with respect to the fast-axes of the PMF 1 and PMF 2. Under this arrangement, the flat-top band mode can be obtained in any path (CW or CCW path). The interleaved flat-top band mode can be implemented by rotating one polarizer (the input polarizer in the CW path or the output polarizer in the CCW path) by $\pi/2$ with other optical elements remained unchanged. In the case of the lossy flat-top band mode, the polarization planes of input and output polarizers form the angles of $2\pi/17$ and $5\pi/102$ in the CW path and the angles of $-56\pi/102$ and $-2\pi/17$ in the CCW path, respectively, with respect to the fast-axes of the PMF 1 and PMF 2. Likewise, the lossy flat-top band mode can be obtained in any path (CW or CCW path) under this arrangement. The interleaved one can also be realized by rotating one polarizer (the input polarizer in the CW path or the output polarizer in the CCW path) by $4\pi/17$ with other optical elements remained unchanged.

As can be found from Table 1 and (3)–(6), our Lyot-type filter can operate in a flat-top band or a lossy flat-top band mode and can be interleaved in each mode by the proper selection of the orientation angles (θ_{h1} and θ_{h2}) of two HWPs. In particular, θ_{h1} and θ_{h2} have an angle symmetry of $\pi/2$ in (2) because the HWP has the intrinsic angle symmetry of π in its azimuth angle. This theoretical calculation is visualized in Fig. 2(a) and (b). Fig. 2(a) shows the calculated transmission spectra of the filter, which are plotted using the transmittances in flat-top and interleaved flat-top band modes given by (3) and (4), respectively. Flat-top and interleaved flat-top band transmission spectra are plotted in orange solid and violet dashed lines, respectively. The transmission spectrum of the conventional SBF is also displayed for comparison in black dash-dotted lines. Fig. 2(b) shows the calculated transmission spectra of the filter in lossy flat-top and interleaved lossy flat-top band modes given by (5) and (6), respectively. Lossy flat-top band transmission spectrum and its interleaved version are plotted in orange solid and violet dashed lines, respectively. In theoretical transmission plots shown in Fig. 2(a) and (b), the PMF birefringence was set as 4.8×10^{-4}, and the length of the PMF 1 was set as 6.25 m so that the wavelength spacing between pass band (channel) centers in the transmission spectrum could be 0.8 nm at 1550 nm for further comparison with measured spectra [to be suggested in Fig. 5(a) and (b)].

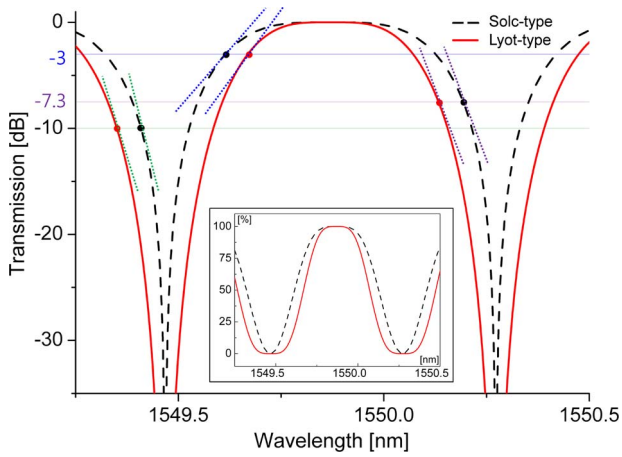

Fig. 3. Comparison of calculated transmission spectra of first-order Solc- and Lyot-type comb filters. The inset shows the same transmission spectra in a linear scale.

For spectral comparison of the Lyot-type comb filter with a Solc-type comb filter of the same order, the calculated transmission spectra of first-order Lyot- and Solc-type comb filters are simultaneously displayed in Fig. 3, which are indicated by red solid and black dashed lines, respectively. Pass band centers of two filters are aligned for convenience. It is clearly seen from the figure that the Lyot-type filter has narrower pass bands in comparison with the Solc-type filter. Further quantitative discussion on the bandwidth will be given later. In particular, the Lyot-type filter shows sharper transition between pass and stop bands than the Solc-type filter does until pass band edges reach a transmission of -7.3 dB ($\sim$18.6%) in the ordinate of Fig. 3. For example, the attenuation rates of Lyot and Solc-type filters are evaluated as $\sim$50.8 and $\sim$43.5 dB/nm at a -3 dB transmission level, or a cutoff level, respectively. The attenuation rate of the Lyot-type filter is $\sim$16.8% higher than that of the Solc-type one at the cutoff level. This attenuation trend is reversed below a transmission level of -7.3 dB, and the attenuation rate of the Solc-type filter becomes $\sim$141.8 dB/nm at a -10 dB transmission level, which is higher by $\sim$11.6% than that of the Lyot-type one. At transmission levels > -7.3 dB, therefore, it can be thought that the Lyot-type filter shows more efficient high-order filtering due to steeper attenuation slopes, compared with the Solc-type one. The narrower and sharper pass band of the filter can be beneficially utilized in reducing unwanted channel noises at spectral locations deviated from a pass band center.

At other combinations of HWP angles except for ones given in Table 1, the Lyot-type filter shows three general transmission modes designated as categories 1, 2, and 3. These categories 1, 2, and 3 exhibit transmission characteristics of 1) a conventional (zeroth-order) SBF with a channel spacing of 0.4 nm except an inherent IL of 1.25 dB, 2) a conventional SBF with a channel spacing of 0.8 nm except an inherent IL of 1.25 dB, and 3) second-order flat-top pass band filter with a channel spacing of 0.8 nm, except for a deteriorated band flatness and IL. Moreover, categories 2 and 3 have interleaved pairs in their transmission spectra. Exemplificative HWP angle combinations for these three categories and corresponding filter transmittances are shown in Table 2. Fig. 4 shows theoretically calculated transmission spectra for three general categories at HWP angle combinations given in Table 2. Categories 1, 2, and 3 are indicated as a solid line, dashed and dotted lines, and dash-dotted and dash-double-dotted lines, respectively. These general cases were also confirmed by experiments.

3. Experimental Results and Discussion

To experimentally verify the calculated results, the Lyot-type comb filter was fabricated by using bow-tie-type PMF (Fibercore HB1250T), a PBS (OZ Optics), and two HWPs (OZ Optics), as shown in Fig. 1. For Lyot-type birefringence combination, the PMF 2 was arranged to be twofold

TABLE 2

Exemplificative HWP angle combinations for three general categories and corresponding transmittances

	θ_{h1}	θ_{h2}	Transmittance
Category 1	$\theta_{p1}/2$	$(\theta_{p1} + \pi/2)/2$	$3(1 - \cos^2\Gamma)/4$
Category 2	$(\theta_{p1} + \pi/6)/2$	$(\theta_{p1} + \pi/3)/2$	$3(\cos\Gamma + 1)/8$
Category 2 (Interleaved)	$(\theta_{p1} - \pi/6)/2$		$-3(\cos\Gamma - 1)/8$
Category 3	$(\theta_{p1} + \pi/3)/2$	$(\theta_{p1} - \pi/6)/2$	$-3(\cos\Gamma + 1)(\cos^2\Gamma - 2)/8$
Category 3 (Interleaved)	$(\theta_{p1} - \pi/3)/2$		$3(\cos\Gamma - 1)(\cos^2\Gamma - 2)/8$

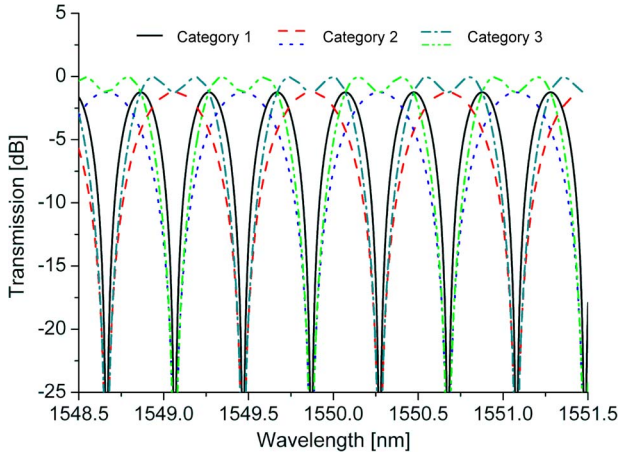

Fig. 4. Theoretically calculated transmission spectra for three general categories.

longer than the PMF 1, and two PMFs were spliced so that their principal axes had a 60° angle offset. The PMF birefringence was $\sim 4.59 \times 10^{-4}$, and the lengths of two PMF segments (PMF 1 and PMF 2) were ~6.25 and ~12.50 m, respectively, which were tailored for the channel spacing of the fabricated filter to be ~0.8 nm at 1550 nm. Splicing points between PMF and single-mode fiber (SMF) or between two PMF segments were marked with diamond symbols in Fig. 1. For the measurement of transmission spectra, an amplified spontaneous emission light source (Fiberlabs FL7004) was used as a nearly unpolarized BBS whose degree of polarization (DOP) was measured as less than 2%, and the transmitted output of the filter was monitored by an OSA (Yokogawa AQ6370C). Fig. 5(a) and (b) show the transmission spectra of the fabricated filter, which are measured in flat-top and lossy flat-top band modes, respectively. In both figures, transmission curves with violet dashed lines are interleaved versions of those with orange solid lines. A flat-top band mode was obtained at an HWP angle set $[\theta_{h1}, \theta_{h2}] = [216°, 126°]$, and its interleaved version at $[\theta_{h1}, \theta_{h2}] = [261°, 126°]$. A lossy flat-top band mode and its interleaved version were obtained at $[\theta_{h1}, \theta_{h2}] = [26°, 49°]$ and $[4°, 49°]$, respectively. Two azimuthal orientation angles $[\theta_{h1}, \theta_{h2}]$ were defined with respect to the horizontal plane of the optical table on which the experiments were carried out. In both modes, the switching displacement between two interleaved curves was measured as ~0.4 nm. As can be seen from Fig. 2(a) and (b), as well as 5(a) and (b), the Lyot-type comb filter can operate in a flat-top band mode or a lossy flat-top band mode, and multiwavelength channels can be interleaved in each mode through the

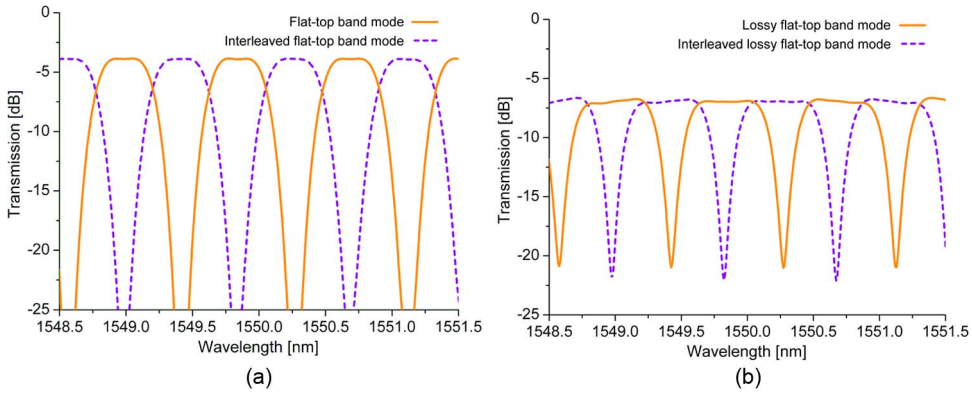

Fig. 5. Measured transmission spectra of (a) flat-top and (b) lossy flat-top band modes. In both flat-top band modes, violet dashed lines indicate interleaved transmission spectra, in comparison with ones indicated as orange solid lines.

adjustment of two HWPs. Considering that the filter transmittance t is a periodical function of θ_{h1} and θ_{h2} with a period of an integer multiple of $\pi/2$, that is, $t(\theta_{h1} + n\pi/2, \theta_{h2} + k\pi/2) = t(\theta_{h1}, \theta_{h2})$ where n and k are integers, θ_{h1} used for the lossy flat-top band mode (t_{lf}) is less than that used for the flat-top band mode (t_f) by 10° $(= 216^\circ - 2 \times 90^\circ - 26^\circ)$, which is deviated by $\sim 1.9^\circ$, and θ_{h2} used for t_{lf} is larger than θ_{h1} used for t_{lf} by 23° $(= 49^\circ - 26^\circ)$, which is deviated by $\sim 0.8^\circ$ in comparison with theoretically predicted angle sets. In addition, θ_{h1} experimentally obtained for $t_{lf,i}$ is less than θ_{h1} for t_{lf} by 22° $(= 26^\circ - 4^\circ)$, which is also deviated by $\sim 0.8^\circ$. The maximum deviation in the HWP angle sets was $\sim 1.9^\circ$.

As predicted in the theoretical calculation, measured transmission spectra provide sufficiently flat-top multi-channel pass bands. The typical spectral flatness of one channel was measured as $<$ 0.06 dB in the flat-top band mode. The spectral flatness in the lossy flat-top band mode was measured as $<$ 0.09 dB at channels near 1550 nm, but it became worse at adjacent channels. The more distant from 1550 nm channels were, the worse their flatness values became. For the pass band of the channel centered at $\sim$1551.55 nm, its spectral flatness was deteriorated into $\sim$0.57 dB. And, the typical extinction ratios of the fabricated filter were measured as $>$ 25.3 dB and $>$ 14.2 dB in the flat-top and lossy flat-top band modes, respectively. At other wavelength bands beyond the spectral range shown in Fig. 5(a), the extinction ratio continues to decrease with the increase of the wavelength deviation from 1550 nm with its value reduced down to 20 dB at wavelengths below 1547 nm or over 1553 nm. The discrepancy between experimental and theoretical HWP angle sets, extinction ratios, or spectral flatness values are mainly caused from tailoring errors of two PMFs, the chromatic phase retardation of two HWPs, and the weak birefringence of SMF segments used to connect optical components comprising the filter [20]. The ILs of the filter were measured as $\sim$3.8 and $\sim$6.5 dB in the flat-top and lossy flat-top band modes, respectively. They mainly come from ILs of two HWPs ($\sim$0.57 and $\sim$0.68 dB) and the PBS ($\sim$1.03 dB for one way, totally $\sim$2.06 dB) including fiber fusion splicing loss between PMF and SMF ($\sim$0.45 dB). The IL can be further reduced by using low-loss polarization controllers or PBSs and by improving the fusion splicing of fiber splices between PMF and SMF.

To make a quantitative comparison between pass band bandwidths of our filter and other comb filters, both 1 and 3 dB pass band bandwidths of a conventional (zeroth-order) SBF, a first-order Solc-type filter [22], and our first-order Lyot-type filter (including the flat-top and the lossy flat-top band modes) were considered. For convenience, figures of merit (FOMs) with respect to 1 and 3 dB bandwidths were defined as 1 dB bandwidth divided by the channel spacing (0.8 nm) and 3 dB bandwidth divided by the same, respectively. With these definitions, in the case of our filter, the 3 dB FOM of the flat-top band mode is calculated as 50%, which is equal to that of the conventional SBF, but the 1 dB FOM is evaluated as 36.4%, which is greater than that of the conventional one, implying a flattened pass band, as shown in Table 3. In the

TABLE 3
Comparison of theoretical and experimental FOMs

	Theoretical FOMs		Experimental FOMs	
	1 dB [%]	3 dB [%]	1 dB [%]	3 dB [%]
Conventional SBF	30.0	50.0	29.1	50.2
1st-order Solc-type filter	47.1	63.6	48.3	64.6
1st-order Lyot-type filter (Flat-top band mode)	36.4	50.0	37.8	52.2
1st-order Lyot-type filter (Lossy flat-top band mode)	61.0	73.2	62.8	75.0

lossy flat-top band mode, its theoretical 3 dB FOM increases up to 73.2%, and its 1 dB FOM is improved more than twice compared with the conventional SBF. In comparison with the first-order Solc-type filter, 1 and 3 dB FOMs at the flat-top band mode of our filter are smaller by 10.7 and 13.6%, respectively, but those at the lossy flat-top band mode are greater by 13.9 and 9.6% at the expense of an IL of $\sim$3.49 dB, respectively. The spectral characteristics obtained in the lossy flat-top band mode provide a bandwidth performance close to that of the second-order Solc-type filter operating in a flat-top band mode, which uses three PMF segments. Experimentally measured FOMs showed similar results. 1 and 3 dB experimental FOMs of the above-mentioned filters were evaluated by using measured values of 1 and 3 dB bandwidths in respective filters [14]. In our Lyot-type filter, the experimental 1 and 3 dB FOMs were measured as $\sim$37.8 and $\sim$52.2% at the flat-top band mode and as $\sim$62.8 and $\sim$75.0% at the lossy flat-top band mode, respectively. There is a difference within 2.2% between measured and calculated FOMs, which can be greatly reduced if two PMF segments are precisely cut so that one segment is two times as long as the other. In addition, in order to investigate the input polarization independence of the Lyot-type filter, which could be theoretically predicted in the mathematical expression of the filter transmittance shown in (2), the polarization sensitivity of the transmission spectrum, that is, polarization-dependent loss (PDL), was measured by placing and adjusting an additional polarization control instrument (Agilent 8169A) in front of the input port of the fabricated filter. The instrument used in the investigation was composed of a rotatable linear polarizer, a quarter-wave plate (QWP), and an HWP, sequentially. During the PDL measurement, we rotated both the QWP and the HWP contained within the instrument in a random way each time, ensuring that the trace of evolved signal polarization had covered the entire Poincare sphere, and the maximum polarization sensitivity was measured as < 0.5 dB, which could be affected by polarization sensitivity of the photodetector and also imperfection of the PBS used in experiments.

4. Spectral Variation of Output SOP

It is intuitively accepted that the SOP_{out} of the Lyot-type comb filter is identical to the SOP_{in} at wavelengths where the filter has transmission maxima. At a given SOP_{in}, the SOP_{out} of the filter will be a function of wavelength, and its spectral variation may be different according to whether the filter operates in the flat-top or the lossy flat-top band mode. The spectral variation of its SOP_{out} can affect the transmission or reflection characteristics of other subsequent optical devices if they are polarization-dependent. In this section, the spectral variation of the SOP_{out} of the filter will be analyzed, and the application of the analysis result will be discussed. To begin with, the spectral variation of the SOP_{out} is investigated within one channel bandwidth at flat-top and lossy flat-top band modes of the filter with respect to several different SOP_{in}'s. Calculated transmission spectra of the filter in flat-top and lossy flat-top band modes, which are plotted in Fig. 6(a) and (b), respectively, show wavelength locations where SOP_{out}'s are analyzed. The

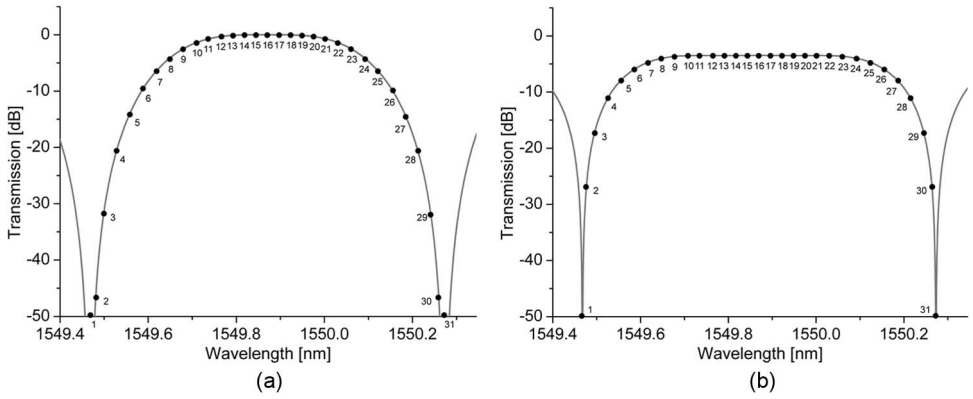

Fig. 6. Calculated filter transmission spectra in (a) flat-top and (b) lossy flat-top band modes, which show wavelength locations where SOP_{out}'s are analyzed. Analysis points are indicated as dots.

analysis points (λ_n) indicated as dots were equally spaced in wavelength, and numbers from $n = 1$ to $n = 31$ were assigned to them with increasing wavelength. The wavelength range utilized for the analysis of the SOP_{out} was from 1549.47 to 1550.27 nm in both flat-top and lossy flat-top band modes.

Fig. 7(a) and (b) show the spectral variation of SOP_{out}'s, obtained at the analysis points set and shown in Fig. 6 with respect to four specific SOP_{in}'s such as 45° linear polarization (LP), 135° LP, right circular polarization (RCP), and left circular polarization (LCP), in flat-top and lossy flat-top band modes, respectively. Filled and empty geometries indicate SOP's that lie on the northern and southern hemispheres of the Poincare sphere, respectively. As can be seen from Fig. 7, the SOP_{out} represents vibrations of ellipses of the same orientation (45° or −45°) whose eccentricity varies from 0 on the equator to ±1 at the north and south poles of the Poincare sphere, respectively. In the flat-top band mode of Fig. 7(a), the SOP_{out} begins with an SOP orthogonal to the SOP_{in} at λ_1 (transmission minimum) and then changes toward the SOP_{in} with increasing wavelength, rotating in a clockwise direction around the axis of LHP on the Poincare sphere. After reaching the SOP_{in} at λ_{16} (pass band center), the SOP_{out} continues to evolve toward the initial SOP that is orthogonal to the SOP_{in}, rotating in the same direction on the Poincare sphere. The SOP_{out} ends up being the initial SOP at λ_{31}, making the spectral period of the SOP_{out} evolution the filter channel spacing. This evolution trend can be found in all four specific SOP_{in}'s. Slightly different situation can be found in the lossy flat-top band mode, as shown in Fig. 7(b). The SOP_{out} starts from the SOP_{in} at λ_1 (transmission minimum) and returns to the SOP_{in} at λ_{16} via an SOP orthogonal to the SOP_{in} at λ_{10}. Then, the same SOP evolution appears once again from λ_{16} to λ_{31}. It is similar to the case of the flat-top band mode that the SOP_{out} varies with increasing wavelength rotating in a clockwise direction around the axis of LHP on the Poincare sphere. But, the SOP_{out} makes two revolutions per channel spacing (from λ_1 to λ_{31}) in this case whereas it makes one revolution per channel spacing in the case of the flat-top band mode. That is to say, the spectral period of the SOP_{out} evolution is a half of the channel spacing in the lossy flat-top band mode. This evolution trend also applies to all four specific SOP_{in}'s likewise. In addition, when the SOP_{in} is LHP or linear vertical polarization (LVP), the SOP_{out} is identical to the SOP_{in} because linearly polarized light introduced into the PBS propagates through the polarization-diversity loop in only one (CW or CCW) direction with only LHP or LVP component coming out of the PBS.

From this wavelength dependence of the SOP_{out}, the Lyot-type filter can exhibit totally different output spectra if a linear polarizer, i.e., an analyzer, is employed and located at its output port, which is worth being examined further. Fig. 8(a) and (b) indicate the calculated transmission spectra with respect to four different specific SOP_{in}'s such as 45° LP, 135° LP, RCP, and LCP with the orientation angle of the analyzer fixed at 45° with respect to the horizontal axis of the PBS in flat-top and lossy flat-top band modes, respectively. As can be seen from the figures,

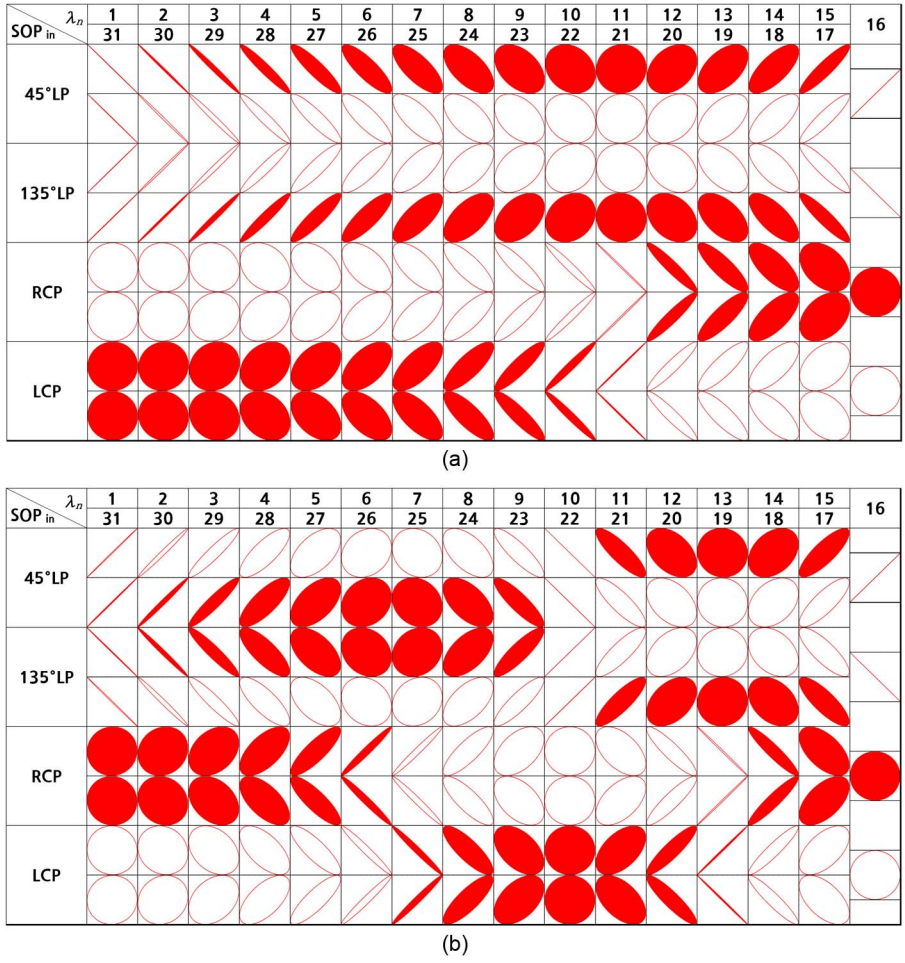

Fig. 7. Spectral variation of SOP_{out}'s, obtained at analysis points shown in Fig. 6 with respect to four SOP_{in}'s such as 45° LP, 135° LP, RCP, and LCP, in (a) flat-top and (b) lossy flat-top band modes. Filled and empty geometries indicate SOP's that lie on the northern and southern hemispheres of the Poincare sphere, respectively.

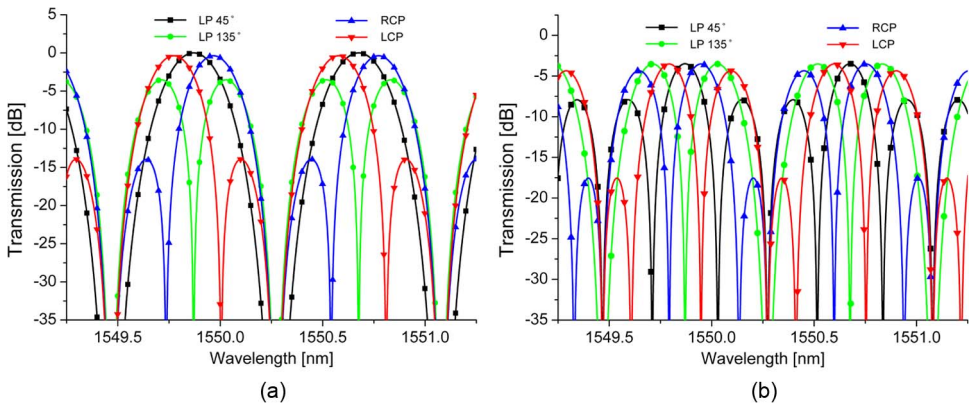

Fig. 8. Calculated transmission spectra with respect to four different SOP_{in}'s such as 45° LP, 135° LP, RCP, and LCP with orientation angle of analyzer, located at filter output port, fixed at 45° in (a) flat-top and (b) lossy flat-top band modes.

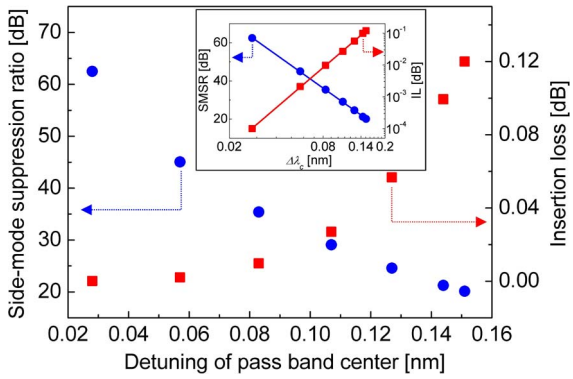

Fig. 9. Theoretical variation of SMSR and IL with respect to wavelength detuning of pass band center.

one or two spectral notches are created within the pass band of the transmission spectrum, which results from the existence of 135° LP in the SOP_{out} and an analyzer orientation angle of 45°. As this notch takes the original flat-top spectrum apart, it weakens filter flatness making the filtering order lower and the pass band shrink, but specific narrow pass bands can be selected within the flat-top band by varying the SOP_{in}. In the flat-top band mode shown in Fig. 8(a), one spectral notch moves from the shorter wavelength dip location (lower edge) to the pass band center of one channel showing redshift, when the SOP_{in} varies from 45° LP to 135° LP via RCP, rotating in a counterclockwise direction around the axis of LHP on the Poincare sphere. With the change of the SOP_{in} from 135° LP to 45° LP via LCP, this notch continues its redshift from the pass band center to the longer wavelength dip location (upper edge) of the channel. At SOP_{in}'s of RCP and LCP, the notch is located at the spectral positions ∼0.27 and ∼0.53 nm distant from the lower edge of one channel, respectively. Ultimately, one counterclockwise revolution of the SOP_{in} on the Poincare sphere makes this spectral notch move to the upper edge and return to its original position restarting from the lower edge within the channel bandwidth, making the total wavelength displacement of the notch the channel spacing (0.8 nm). In the lossy flat-top band mode in Fig. 8(b), the SOP_{in} variation from 45° LP to 135° LP via RCP (through counterclockwise rotation around the axis of LHP on the Poincare sphere) makes two spectral notches with a certain wavelength separation simultaneously redshift until shorter and longer wavelength notches reach the pass band center and upper edge of one channel, respectively. Then, the SOP_{in} variation from 135° LP to 45° LP via LCP causes them to continue their redshift until one of two notches arrives at the wavelength position where the other is initially located at an SOP_{in} of 45° LP. At an SOP_{in} of RCP, shorter and longer wavelength notches are located at two spectral positions ∼0.32 and ∼0.66 nm distant from the lower edge of one channel, respectively. In the case of an SOP_{in} of LCP, they take their spectral positions ∼0.14 and ∼0.48 nm distant from its lower edge. Consequently, when the SOP_{in} makes one counterclockwise revolution around the axis of LHP on the Poincare sphere, two spectral notches redshift until one of them arrives at the wavelength position where the other is initially located, making the sum of their spectral displacements the channel spacing (0.8 nm).

As can be seen and explained from Fig. 8, specific spectral portions of a flat-top pass band (channel) of the Lyot-type filter could be passed or rejected by controlling the SOP_{in} with the help of an analyzer, resulting in a shrunk pass band. In particular, in the case of the flat-top band mode, the center wavelength of the shrunk pass band can be continuously and minutely tuned through the fine control of the SOP_{in} in a narrow wavelength range. Fig. 9 shows the theoretical variation of the SMSR and the IL with respect to the wavelength detuning $\Delta\lambda_c$ of the pass band center in the Lyot-type comb filter with the analyzer located at its output port. The SMSR and the IL show monotonic decrease and increase with increasing wavelength detuning $(\Delta\lambda_c)$, respectively, and it is also found out from the inset of Fig. 9 that the SMSR has a logarithmic relationship with $\Delta\lambda_c$, and the IL is a fractional power of $\Delta\lambda_c$ with a fractional exponent

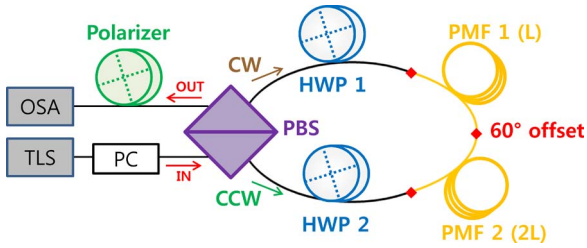

Fig. 10. Schematic diagram of experimental setup for analyzing spectral variation of SOP_{out}.

of ∼4.19. The relationship between the SMSR (y_1) and $\Delta\lambda_c$ can be formulated as $y_1 = a \cdot \log(\Delta\lambda_c) + b$ where constants a and b are approximately -58.03 and -27.41, respectively. And the relationship between the IL (y_2) and $\Delta\lambda_c$ can also be formulated as $y_2 = c \cdot (\Delta\lambda_c)d$ where constants c and d are ∼329.51 and ∼4.19, respectively. This theoretical prediction suggests that the fine and continuous center wavelength tuning of the shrunk pass band is possible in a limited wavelength range corresponding to ∼12.81% of the channel spacing with an IL and an SMSR kept as less than 0.023 dB and more than 30 dB, respectively. The wavelength tuning range of the shrunk pass band can be further increased up to ∼19.05% of the channel spacing at the expense of the IL ($<$ 0.124 dB) and the SMSR ($>$ 20 dB).

In order to verify the theoretical prediction of the SOP_{out} of the Lyot-type filter, the spectral variation of the SOP_{out} was observed by using a coherent light source and an output linear polarizer (analyzer) shown in Fig. 10. A tunable laser (ANDO AQ4321D) with a wavelength tuning range of 1520–1620 nm was employed as a coherent light source, and an additional PC was utilized to control the SOP_{in} of the filter. The lasing wavelength of the tunable laser source (TLS) linked with the OSA was swept for the measurement of filter transmission spectra, and typical sweep time was ∼1 s per sweep for a wavelength range of 5 nm. The linewidth and the SMSR of the TLS were 200 kHz and $<$ 45 dB, respectively. In case the BBS is used instead of the TLS, the DOP of output light coming out of the PBS of the filter becomes very low due to short coherence length (a few millimeters) of amplified spontaneous emission light, and output light seems nearly unpolarized, which is likely to make it difficult to observe the spectral dependence of the SOP_{out}. In the determination of the SOP_{in} (before the input port of the filter), it can be regarded as LHP when vertical one of two polarization components emerging from the PBS becomes zero, and *vice versa*. Circular polarization such as RCP and LCP can be identified with an additional rotatable linear polarizer as circularly polarized light passes through the linear polarizer with an IL of 3 dB irrespective of the polarizer orientation, showing invariant output power with the polarizer arbitrarily rotated. The analyzer allows the transmission of light with only LP aligned along its polarization axis, and light with other SOPs except the above LP passes through the analyzer with its optical power decreased according to Malus' law. Polychromatic light with wavelength-dependent SOPs has spectrally different optical transmission when passing through the analyzer, and thus the output spectrum of the analyzer can be used to infer the SOP_{out} of the Lyot-type filter at a specific wavelength when compared with the original spectrum obtained without the analyzer.

Fig. 11(a) and (b) show transmission spectra measured with respect to four different SOP_{in}'s such as 45° LP, 135° LP, RCP, and LCP with an analyzer fixed at an azimuthal angle of 45° in flat-top and lossy flat-top band modes, respectively. As predicted in Fig. 8, it was observed that one or two spectral notches appeared making flat-top pass band be shrunk and moved according to the variation of the SOP_{in} selecting specific narrow pass bands. In the flat-top band mode shown in Fig. 11(a), a spectral notch showed redshift, moving from the lower edge to the pass band center of one channel with the variation of the SOP_{in} from 45° LP to 135° LP via RCP. With the change of the SOP_{in} from 135° LP to 45° LP via LCP, this notch continued to move from the pass band center to the upper edge of the channel. At SOP_{in}'s of RCP and LCP, the notch was located at the spectral positions ∼0.26 and ∼0.54 nm distant from the lower edge of the channel, respectively. One cyclic variation of the SOP_{in}, which started from 45° LP and

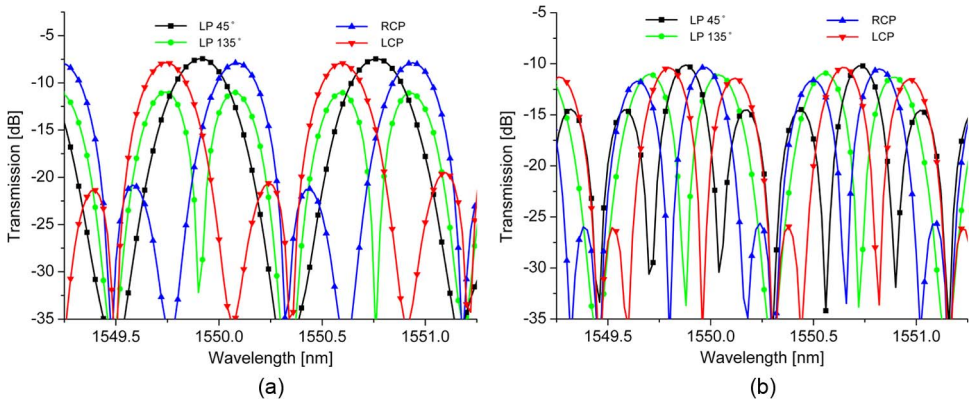

Fig. 11. Transmission spectra measured with respect to four different SOP_{in}'s with orientation angle of analyzer fixed at 45° in (a) flat-top and (b) lossy flat-top band modes.

returned to 45° LP via RCP, 135° LP, and LCP, made a spectral notch move from the lower edge to the upper edge of one channel, i.e., be swept by the amount of the channel spacing (∼0.8 nm) within the channel bandwidth. In the lossy flat-top band mode shown in Fig. 11(b), with the variation of the SOP_{in} from 45° LP to 135° LP via RCP, two spectral notches with a certain wavelength interval also showed redshift, moving simultaneously until shorter and longer wavelength notches reached the pass band center and upper edge of one channel, respectively. Then, the SOP_{in} variation from 135° LP to 45° LP via LCP made them to keep their redshift until one of them arrived at the wavelength position where the other was initially located at an SOP_{in} of 45° LP. It was observed that at an SOP_{in} of RCP shorter and longer wavelength notches took their spectral positions ∼0.33 and ∼0.69 nm distant from the lower edge of one channel, respectively. In the case of an SOP_{in} of LCP, they were observed to be located at spectral positions ∼0.14 and ∼0.49 nm distant from its lower edge. Similarly, one cyclic variation of the SOP_{in}, which started from 45° LP and returned to 45° LP via RCP, 135° LP, and LCP, made two spectral notches redshift until one of them arrived at the wavelength position where the other was initially located, allowing them to be swept within the channel bandwidth with the sum of their swept wavelength to be the channel spacing (∼0.8 nm). In addition, spectral dips, which are slightly dull compared with the theoretical results, seem to be caused by the low wavelength resolution of the TLS, which is automatically set and fixed when linked with the OSA, and the finite extinction ratio of the non-ideal polarizer used in the experiment. As a result, by harnessing the spectral dependence of the SOP_{out} and employing an analyzer, specific spectral portions of a flat-top pass band (channel) of the Lyot-type comb filter could be passed or rejected, and the pass band center could be finely tuned by controlling the SOP_{in}. Spectral notches obtained here can be also applied to suppress unwanted spectral components in modulated optical signals.

5. Conclusion

In summary, we investigated the transmission and output polarization properties of the first-order Lyot-type fiber comb filter based on the PDLS. The first-order Lyot-type filter was composed of a PBS, two HWPs, and two PMF segments. Two PMF segments were concatenated with a 60° offset between their principal axes, and one of them was two times longer than the other. The filter transmittance was theoretically calculated, and the theoretical prediction was verified by experimental demonstration. By controlling two HWPs, the filter could operate in the flat-top or the lossy flat-top band mode, and its multiwavelength channels could be interleaved in both modes, which could not be obtained in the previous Lyot-Sagnac comb filter. In addition, the filter showed sharper transition between pass and stop bands in comparison with a PDLS-based Solc-type comb filter with the same order. In particular, the SOP_{out} of the filter was theoretically and experimentally examined. The SOP_{out} of the filter showed wavelength-dependent evolution, rotating in

a clockwise direction around the axis of LHP on the Poincare sphere with increasing wavelength. The spectral periods of the SOP_{out} evolution were the channel spacing of the filter and its half in flat-top and lossy flat-top band modes, respectively, with SOP_{out}'s at pass band centers (transmission maxima) kept as an SOP_{in}. With the help of the analyzer, some spectral portion of a channel could be passed or rejected by controlling input polarization, resulting in a shrunk narrow pass band. In addition, in the flat-top band mode, it was theoretically predicted that the fine and continuous center wavelength tuning of the shrunk pass band was possible in a limited wavelength range corresponding to $\sim$12.81% of the channel spacing with an IL and an SMSR kept as less than 0.023 dB and more than 30 dB, respectively. This wavelength tuning range could be increased up to $\sim$19.05% of the channel spacing at the expense of the IL ($<$ 0.124 dB) and the SMSR ($>$ 20 dB).

References

[1] T. Hasegawa, K. Inoue, and K. Oda, "Polarization independent frequency conversion by fiber four-wave mixing with a polarization-diversity technique," *IEEE Photon. Technol. Lett.*, vol. 5, no. 8, pp. 947–949, Aug. 1993.

[2] T. Morioka, K. Mori, and M. Saruwatari, "Ultrafast polarization-independent optical demultiplexer using optical carrier frequency shift through crossphase modulation," *Electron. Lett.*, vol. 28, pp. 1070–1072, 1992.

[3] Y. W. Lee, K. J. Han, J. Jung, and B. Lee, "Polarization-independent tunable fiber comb filter," *IEEE Photon. Technol. Lett.*, vol. 16, no. 9, pp. 2066–2068, Sep. 2004.

[4] Y. W. Lee, K. J. Han, B. Lee, and J. Jung, "Polarization-independent all-fiber multiwavelength-switchable filter based on a polarization-diversity loop configuration," *Opt. Exp.*, vol. 11, no. 25, pp. 3359–3364, Dec. 2003.

[5] G. Zhu, Q. Wang, H. Chen, H. Dong, and N. K. Dutta, "High-quality optical pulse train generation at 80 Gb/s using a modified regenerative-type mode-locked fiber laser," *IEEE J. Quantum Electron.*, vol. 40, pp. 721–725, Jun. 2004.

[6] X. Fang, K. Demarest, H. Ji, C. Allen, and L. Pelz, "A subnanosecond polarization-independent tunable filter/wavelength router using a Sagnac interferometer," *IEEE Photon. Technol. Lett.*, vol. 9, no. 11, pp. 1490–1492, Nov. 1997.

[7] G. Rossi, O. Jerphagnon, B. Olsson, and D. J. Blumenthal, "Optical SCM data extraction using a fiber-loop mirror for WDM network systems," *IEEE Photon. Technol. Lett.*, vol. 12, no. 7, pp. 897–899, Jul. 2000.

[8] Z. Jia, M. Chen, K. Xu, Y. Dong, and S. Xie, "Performance analysis of optical label eraser," *Opt. Commun.*, vol. 205, no. 4/6, pp. 265–269, May 2002.

[9] I. Yoon, Y. W. Lee, J. Jung, and B. Lee, "Tunable multiwavelength fiber laser employing a comb filter based on a polarization-diversity loop configuration," *J. Lightw. Technol.*, vol. 24, no. 4, pp. 1805–1811, Apr. 2006.

[10] C. S. Kim and J. U. Kang, "Multiwavelength switching of Raman fiber ring laser incorporating composite polarization-maintaining fiber Lyot-Sagnac filter," *Appl. Opt.*, vol. 43, no. 15, pp. 3151–3157, 2004.

[11] Y. W. Lee, J. Jung, and B. Lee, "Multiwavelength-switchable SOA-fiber ring laser based on polarization-maintaining fiber loop mirror and polarization beam splitter," *IEEE Photon. Technol. Lett.*, vol. 16, pp. 54–56, Jan. 2004.

[12] M. P. Fok, K. L. Lee, and C. Shu, "Waveband-switchable SOA ring laser constructed with a phase modulator loop mirror filter," *IEEE Photon. Technol. Lett.*, vol. 17, no. 7, pp. 1393–1395, Jul. 2005.

[13] X. Fang and R. O. Claus, "Polarization-independent all-fiber wavelength-division multiplexer based on a Sagnac interferometer," *Opt. Lett.*, vol. 20, no. 20, pp. 2146–2148, Oct. 1995.

[14] Y. W. Lee, H. Kim, J. Jung, and B. Lee, "Wavelength-switchable flat-top fiber comb filter based on a Solc type birefringence combination," *Opt. Exp.*, vol. 13, no. 3, pp. 1039–1048, Feb. 2005.

[15] Y. W. Lee, H. Kim, and Y. W. Lee, "Second-order all-fiber comb filter based on polarization-diversity loop configuration," *Opt. Exp.*, vol. 16, no. 6, pp. 3871–3876, Mar. 2008.

[16] Z. Jia, M. Chen, and S. Xie, "Label erasing technique employing Lyot-Sagnac filter," *Electron. Lett.*, vol. 38, no. 24, pp. 1563–1564, Nov. 2002.

[17] I. Solc, "Birefringent chain filters," *J. Opt. Soc. Amer.*, vol. 55, no. 6, pp. 621–625, 1965.

[18] Z. Yan *et al.*, "All-fiber polarization interference filters based on 45°-tilted fiber gratings," *Opt. Lett.*, vol. 37, no. 3, pp. 353–355, 2012.

[19] X. Fang and K. Demarest, "A compound high-order polarization-independent birefringence filter using Sagnac interferometers," *IEEE Photon. Technol. Lett.*, vol. 9, no. 4, pp. 458–460, Apr. 1997.

[20] S. Jo, K. Park, and Y. W. Lee, "Lyot-type flat-top fibre multiwavelength filter based on polarisation-diversity loop structure," *Micro Nano Lett.*, vol. 9, pp. 858–861, Dec. 2014.

[21] R. C. Jones, "A new calculus for the treatment of optical systems," *J. Opt. Soc. Amer.*, vol. 31, no. 7, pp. 488–493, 1941.

[22] Y. Kim and Y. W. Lee, "Study on spectral deviations of high-order optical fiber comb filter based on polarization-diversity loop configuration," *Opt. Commun.*, vol. 301/302, pp. 159–163, Aug. 2013.